Higher Order Active Contours and their Application to the Detection of Line Networks in Satellite Imagery

Marie Rochery, Ian Jermyn, Josiane Zerubia

Ariana (joint research group CNRS/INRIA/UNSA)
INRIA, B.P. 93, 06902 Sophia Antipolis cedex, France
e-mail: (marie.rochery, ian.jermyn, josiane.zerubia)@inria.fr

Abstract

We present a novel method for the incorporation of shape information into active contour models, and apply it to the extraction of line networks (*e.g.* road, water) from satellite imagery. The method is based on a new class of contour energies. These energies are quadratic on the space of one-chains in the image, as opposed to classical energies, which are linear. They can be expressed as double integrals on the contour, and thus incorporate non-trivial interactions between different contour points. The new energies describe families of contours that share complex geometric properties, without making reference to any particular shape. Networks fall into such a family, and to model them we make a particular choice of quadratic energy whose minima are reticulated. To optimize the energies, we use a level set approach. The forces derived from the new energies are non-local however, thus necessitating an extension of standard level set methods. Promising experimental results are obtained using real images.

1 Introduction

Active contours have been extensively used in computer vision since the original paper of Kass *at al.* [18]. They have proved their efficiency in many application domains, including image segmentation, video tracking, inpainting, and 3D reconstruction. The idea is simple and attractive: define an 'energy' functional on a space of curves in the image domain, designed so that the (local) minima of the energy delineate features or objects of interest in the image; then find a minimum. The number of variations on this theme is enormous. The original active contours were defined on the space of parameterized open or closed curves in the image domain [18, 8], and penalized irregularity, and low image gradients under the curve. However the parameterization dependence of these models is undesirable, and in consequence most subsequent active contour models have been defined as functionals on the space of equivalence classes of curves under changes of parameterization. 'Geometric' or 'geodesic' active contours [23, 3, 4, 19] constitute one example. A metric is defined on the image domain, and curve length in this metric is then used as the energy functional. Region terms were added to the energy, in [26, 5, 15] among others, to facilitate the description of region properties, and to reduce sensitivity to noise and clutter. On the algorithmic side, early methods for finding a minimum used gradient descent on the contour itself, but problems with parameterization and topology change led to the adoption of level set methods [25], which do not require the former and allow the latter.

In all these models, the *a priori* constraints on the contour rely on elasticity (and sometimes rigidity) measures. These geometrical constraints lead to curvature-based regularization forces that are generic in the sense of encouraging circles as the energy minima. Recently, several approaches have been developed that incorporate more detailed geometric information about the target object.

Leventon *et al.* [22] incorporate shape information into the evolution of geodesic active contours. The contour is evolved in the direction of an estimated shape and pose. The shape of the target object is represented by a signed distance function, and deviations from the mean distance function are penalized. Cremers *et al.* [11] modify the Mumford-Shah functional to incorporate statistical shape knowledge. They use an explicit parameterization of the contour as a closed spline curve, and learn a Gaussian probability distribution for the spline control point vectors. The statistical prior restricts the contour deformations to the subspace of learned deformations.

Paragios and Rousson [27] propose a functional that can account for the global and local shape properties of the target object. A prior shape model is built using aligned training examples. A probabilistic framework uses the shape image and the variability of shape deformations as unknown variables. They seek a global transformation and a level set representation that maximizes the posterior probability given the prior shape model. Chen *et al.* [7] define an energy functional depending on the gradient and the average shape of the target object. The prior shape term evaluates the similarity of the shape of the contour (modulo scale, rotation and translation) to that of the reference shape through the computation of a distance function using the Fast Marching method of Sethian [31].

If one were to summarize the way in which the above methods describe shape, it would be as follows. Given one or more training examples, and a shape representation, a 'mean' shape is computed. (For the difficulties inherent in doing this, see [16].) In addition, a covariance matrix is either assumed (to be the identity), or computed as the data covariance of a finite number of 'principal modes of variation' of the shape. An energy/distance term can then be constructed: it is essentially the logarithm of a Gaussian distribution, with the given mean and covariance. Plainly this encourages the properties of the contour summarized by the shape space, to approach the given mean.

In contrast, we would like to introduce shape information that is not specific to a particular or single object, but that rather defines a large class of shapes that share a 'family' resemblance. To give an example pertinent to the work presented here: what is it that all road networks have in common geometrically? Clearly they are not Gaussian variations around a mean parameterized by a few simple geometrical quantities. On the other hand, they clearly share a number of properties, some of which lead us to apply the word 'network' to them.

To model such shape families, we propose a new *class* of active contour models. In these models, the contour interacts with itself. That is, the models describe interactions or correlations between different points of the contour, something entirely absent from conventional models. These interactions in their turn allow the incorporation of non-trivial geometric information into prior terms, and in particular the description of shape families such as networks. If used as data terms, they allow the description of more complex relations between the contour and the image.

1.1 One-chains

In order to clarify the nature of the new models, it is helpful to use the notion of a 'one-chain'. The space of one-chains $\mathcal{C}_1(X)$ in a manifold X is the space of all formal linear combinations of curves in that manifold. Active contour energies are functionals on this space. In practice however, we are interested only in closed one-chains with binary coefficients, which correspond to closed curves with no repeated segments, so that minimization of the energy is constrained to this subset, $\tilde{\mathcal{C}}_1(X)$.

Single integrals of quantities along a curve are then linear functionals on $\mathcal{C}_1(X)$: the integral along two curves taken together is the sum of the integrals along each of them taken separately. Almost all previous models use energies that are linear in this sense.[1] The consequence is that these energies are local: they can describe interactions only between infinitesimally separated points of the contour, because an integral is essentially a sum over single points.

It is however possible to define *higher-order* functionals on $\mathcal{C}_1(X)$. These functionals are expressed as *multiple* integrals (two in the case of quadratic energies) and can hence describe interactions between arbitrary points of the curve, because the multiple integral constitute a sum over all tuples of points (pairs in the case of quadratic energies).

Such higher-order functionals can be used to define *higher-order* active contours. As explained above, these models bear the same relation to conventional active contours as polynomials bear to linear functions, and enlarge the range of possible models in a similar fashion. (As we will see in the next section, there are only two Euclidean-invariant linear energies, but a whole function space full of Euclidean-invariant quadratic energies.)

The above can be seen from another point of view. Given an energy E on some set V, we can (at least formally) define a probability distribution as the normalized negative exponential of E: $\Pr(v) = Z^{-1} \exp -E(v)$. If the set V is a vector space, and if E is a linear functional, we have an exponential distribution. For an exponential distribution, the components of v in any basis are independent. In the case of one-chains on a manifold X, this means that the points of the contour are independent. Apart from the trivial dependency of closure, this independence necessarily survives the conditioning of the probability distribution on membership of the subset $\tilde{\mathcal{C}}_1(X)$ (although it no longer makes sense to describe it as exponential, since $\tilde{\mathcal{C}}_1(X)$ is not a vector space).

By contrast, if the energy E is quadratic or higher-order, the components of v are not necessarily independent (and even if they are, the behaviour is still not linear). Correlations now exist between the components. Focusing on the quadratic case, the distribution becomes Gaussian on $\mathcal{C}_1(X)$. It is not however 'Gaussian' on $\tilde{\mathcal{C}}_1(X)$. Indeed such a description would not make sense since $\tilde{\mathcal{C}}_1(X)$ is not a vector space, and it is thus important to realize the great difference between the Gaussian distributions used in the works cited earlier, and the Gaussian distribution resulting from a quadratic active contour.

To see the difference, consider by analogy a two-dimensional vector space, *i.e.* the plane (analogous to $\mathcal{C}_1(X)$), and a curve in that space (analogous to $\tilde{\mathcal{C}}_1(X)$). The works cited above approximate a probability distribution on the curve by choosing a point (the 'mean') and constructing a Gaussian distribution in some coordinate distribution centred on that point, essentially treating the curve as if it were an infinite straight line. In contrast, the Gaussian distribution resulting from a quadratic active contour energy is analogous to a Gaussian distribution *on the plane*, which is then restricted to the curve by conditional probability. The nature of the distribution on the curve can then be very much more complicated than in the previous case, and indeed the two notions of 'Gaussian' have little to do with one another.

The new energies require new minimization techniques too. Higher-order energies lead to non-local forces: the force at a point in the contour depends on the global configuration of the contour and not just on its infinitesimal neighbour-

[1] All those previous energies that are not linear are nevertheless built of linear functionals, in the sense of being products or quotients [17, 15] of them.

hood. The computation of the force thus involves integrals over the contour. We will use a level set approach, and in the process we will extend standard methods to handle non-local forces in a way similar to, but necessarily more precise than, that used for incompressible (*i.e.* area preserving) flows.

In sections 2 and 3, we describe the new class of active contour energies and present the level set method we use to minimize them. In section 4, we apply a particular quadratic energy functional to the extraction of line networks in satellite imagery. In section 5, we present experimental results. We summarize and conclude in section 6.

2 Energy Functional

We first discuss conventional linear energies to establish concepts and notation, and then the construction and nature of quadratic energies.

2.1 Linear Energies

Let Ω be a bounded subset of $\mathbb{R}^2$, and $I : \Omega \to \mathbb{R}$ be an image. The discussion below applies to general 1-chains, but for ease of presentation, we will consider a map $C : S^1 \to \Omega$. Given a metric g and a function f on Ω, both of which may depend on I, the following linear functional on the space of 1-chains can be defined:

$$E(C) = \int_{S^1} \star_{C^*g} C^* f \quad . \tag{1}$$

Here, C^* is pullback by C, C^*g is therefore the metric on S^1 induced by C, and $\star_{C^*g}$ is the associated Hodge star. This equation manifests the invariance of the energy both to changes of coordinates on Ω and S^1, and to changes in C that result in the same geometric curve in Ω (diffeomorphism invariance). By choosing a coordinate p on S^1, we find the more familiar expression

$$E(C) = \oint dp \ |\vec{\mathbf{t}}(p)|_g \ f(C(p)) \ , \tag{2}$$

where $\vec{\mathbf{t}}(p) = C'(p)$ is the tangent vector to C at p, and $|v|_g$ is the norm of the vector v in the metric g. The form of functional in equations (1) and (2) encompasses most of the models that have been used in the past. Another linear possibility is to integrate a 1-form A (intuitively, a vector field) over the 1-chain:

$$E(C) = \int_{S^1} C^* A = \oint dp \ \vec{\mathbf{t}}(p) \cdot A \ , \tag{3}$$

where $v \cdot A$ is the 'inner product' of the 1-form A and vector v. The area of the interior of a 1-chain is one example.

If the metric, function and 1-form do not depend on the image, it is natural to enforce Euclidean translation and rotation invariance. This forces f to be constant, g to be invariant (*i.e.* Euclidean) and A to calculate the interior area. Thus there are only two linear terms compatible with Euclidean invariance: length and area.[2]

2.2 Quadratic energies

The formal construction of quadratic energies proceeds as follows. Given two 1-chains C and D in Ω, one can define their product, $C \otimes D$, a 2-chain in Ω^2. (In the case that $C : S^1 \to \Omega$, this construction gives the map $C \times C : T^2 \to \Omega^2$, where $T^2 = S^1 \times S^1$ is the 2-torus.) We thus have a map $\otimes : \mathcal{C}_1(\Omega) \times \mathcal{C}_1(\Omega) \to \mathcal{C}_2(\Omega^2)$, where $\mathcal{C}_p(X)$ is the space of p-chains in the manifold X. A linear functional on $\mathcal{C}_2(\Omega^2)$ becomes a bilinear functional on $\mathcal{C}_1(\Omega) \times \mathcal{C}_1(\Omega)$ by this construction. In turn, by definition, such a bilinear functional is, when composed with the diagonal map $\mathcal{C}_1(\Omega) \to \mathcal{C}_1(\Omega) \times \mathcal{C}_1(\Omega) : C \mapsto (C, C)$, a *quadratic* functional on $\mathcal{C}_1(\Omega)$.

Thus to construct a quadratic functional on the space of 1-chains in Ω, we must construct a linear functional on the space of 2-chains in Ω^2. As in section 2.1, we can do this in two ways. Given a metric and a function on Ω^2, we may define a functional on 2-chains analogous to equation (1). These functionals are interesting to consider, but space requirements prevent us from discussing them further here. Alternatively, we may define a 2-form F on Ω^2, and use the analogue of equation (3):

$$E(C) = \int_{T^2} (C \times C)^* F \quad . \tag{4}$$

The product structures of $C \times C$ and T^2 mean that this functional can always be written (in terms of coordinates (p, p') on T^2) as

$$E(C) = \int_{T^2} dp \, dp' \ \vec{\mathbf{t}}(p) \cdot F(C(p), C(p')) \cdot \vec{\mathbf{t}}(p') \ , \tag{5}$$

where $F(x, x')$, for each $(x, x') \in \Omega^2$, is a matrix. The operator F allows us to model a non-trivial interaction between different contour points. Note that this interaction is not Markov since the interaction is mediated by the embedding rather than the embedded space. The forces derived from the energy in equation (5) are non-local: the force at a point is determined by an integral over the contour.

If the 2-form F does not depend on the image, then we again require the energy to be Euclidean invariant. This results in the form

$$E(C) = -\oint \oint dp \, dp' \ \vec{\mathbf{t}}(p) \cdot \vec{\mathbf{t}}(p') \ \Psi(|C(p) - C(p')|) \ , \tag{6}$$

where $|x - y|$ is the Euclidean distance between points x and y in Ω. The function Ψ weights the interactions between different points of the curve according to their distance, and

[2] We will not consider here energy terms that depend on the curvature. These involve lifting the 1-chain C to the tangent bundle of Ω, but otherwise the mechanics of the construction of functionals is the same as here.

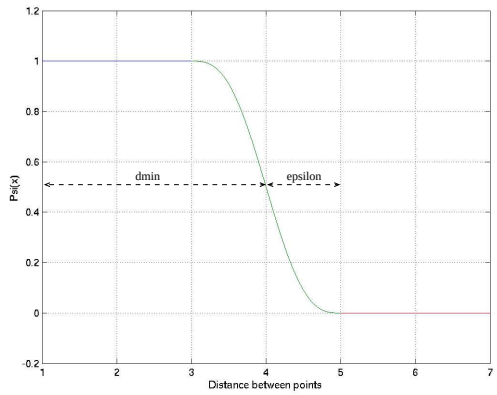

Figure 1: The function Ψ

must be chosen carefully since it defines the geometrical content of the model. In order to eliminate uncontrollable size effects, $\Psi(x)$ should tend to zero as x tends to infinity, meaning that two far away points do not interact. It should also be chosen so that the integral converges. Otherwise, any choice of Ψ is possible, but the detailed behaviour to be expected from any particular choice is far from obvious and remains to be studied.

In the experiments shown later, we use the following form for Ψ:

$$\Psi(x) = \begin{cases} 1 \text{ if } x < d_{\min} - \epsilon \\ 0 \text{ if } x > d_{\min} + \epsilon \\ \frac{1}{2}(1 - \frac{x - d_{\min}}{\epsilon} - \frac{1}{\pi} sin(\pi \frac{x - d_{\min}}{\epsilon}) \text{ otherwise} \end{cases} , \tag{7}$$

where the parameters $d_{\min}$ and ϵ are illustrated on figure 1.

This choice describes a 'hard core' potential between every pair of points with anti-parallel tangent vectors. One of its effects is to prevent two points with anti-parallel tangent vectors from approaching closer than $d_{\min}$. On the other hand, pairs of points with parallel tangent vectors are favoured, thus encouraging straight lines to lengthen. The energy minima that result consist of elongated structures ('arms') of a fixed minimum width that tend to grow. The arms are mutually repulsive, so that they distribute themselves over the domain Ω, and have a limited branching number.

In an earlier model [29], we used another function Ψ:

$$\Psi(x) = \sinh^{-1}(1/x) + x - \sqrt{(}1 + x^2) \ . \tag{8}$$

This function is also decreasing, behaving as $1/2x$ when $x >> 1$ and as $\ln(2/x)$ when $x < 1$, the latter behaviour preventing the integral from diverging. This choice also favours the formation of thin elongated structures, but the divergence of Ψ as x tends to zero causes stability difficulties in calculating the force numerically. Moreover, due the relatively slow decrease of Ψ over a long range, the width of the arms varies considerably more than with the Ψ in equation (7).

The growth away from a circle towards a labyrinthine structure with elongated 'arms' can be understood as follows. A linear analysis of the stability of the circle to small sinusoidal perturbations shows that above a certain angular wavelength, the perturbations, rather than being damped back to zero, are amplified, their size and their spatial frequency around the initial circle being controlled by the Ψ function. Thus instead of smoothing all irregularities, as in the linear case, this energy allows some of them to develop, and hence encourages complex shapes. An uncontrollable instability at all frequencies is prevented by the fact that the 'bumps' corresponding to two peaks in the sinusoid cannot approach closer than $d_{\min}$. Once created, the bumps elongate into arms with parallel sides, thus decreasing the energy, although this nonlinear behaviour can no longer be described within the linear approximation used to study stability. In an infinite domain it seems likely that the energy is not bounded below, and that the arms will continue to grow and to ramify indefinitely. In a finite domain such as an image, this cannot happen due to the repulsion between the arms.

One can view the formation of complex shapes as a case of 'symmetry breaking'. The minima of the Euclidean invariant linear functionals described above, being circles, possess the same symmetries as the energy, but the same is not true in general of quadratic energies. Although the energy may be Euclidean invariant, the minima in general possess no symmetries.

3 Minimization of the energy

In order to minimize the energy, we will use gradient descent, evolving the contour using the level set framework introduced by Osher and Sethian [25]. As is well known, level set representations handle changes of topology naturally, are parameter free, and allow the simple expression of geometrical quantities like curvature. If the contour propagates along the outward normal direction with speed $F(p)$, the level set function obeys

$$\frac{\partial \phi}{\partial t} = F|\nabla \phi| \ . \tag{9}$$

We use the Fast Marching method [31] for the initialization of the function ϕ as a signed distance function and the Narrow Band algorithm [32] to evolve ϕ. This consists of evolving the function only in the narrow band around the zero level set for which $\phi(x, y) < t$, where t is a threshold. This results in significant gains in computational efficiency.

The function F, initially defined only on the contour, is required in equation (9) to be defined all over Ω. In the case that F on the contour can be expressed as a local functional of ϕ, this is easily done by assuming that this definition holds everywhere. For a quadratic energy however, the force at each point of the contour is given by an integral over the whole contour. To calculate the force at a point x_0 then, one could extract the level set corresponding to $\phi(x_0)$ and integrate around it. This process would need to be repeated for

each point in the Narrow Band, and is thus not very efficient. Another way would be to persevere with a pure level set approach, replacing $\oint dp$ by $\int dx\ dy\ \ \delta(\phi, \phi(x_0))|\nabla\phi|$ in the expression of the force, as was done in [6] for incompressible flows. We have found that this technique does indeed work well for area preserving evolutions, but that it is not precise enough for the case at hand. We rather adopted a two-step method: in step one, the $\phi = 0$ contour is extracted and the force is computed at each point by integrating over the contour. In step two, the force is extended over the Narrow Band. It proved necessary to be as precise as possible in these computations. Many of the techniques we tried worked well for area-preserving flows, which also involve integrals over the contour, but failed when it came to quadratic functionals. Note that the contour is used only to compute the force, and not to evolve or represent the contour, so that we lose none of the advantages of the level set method.

In step one, the goal is to extract a list of points $\{C(p_i) = (x_i, y_j)\}$ representing the contour, given the values of the function ϕ at the grid points. This is done, as in [33], by using an Essentially Non Oscillatory polynomial interpolation technique to find the zeros between each pair of neighbouring grid points, coupled with a sophisticated contour tracing algorithm. Any geometrical and image quantities needed to compute the force at the contour points are bilinearly interpolated from the grid. We then compute the force F at each contour point using standard integration techniques.

In step two, we must extend the force F from the zero level set to each grid point in the Narrow Band. We do this using the partial differential equation proposed in [28]. We solve

$$F_\tau + \text{sgn}(\phi)\frac{\nabla\phi}{|\nabla\phi|} \cdot \nabla F = 0 \ \ , \tag{10}$$

where sgn is the sign function, subject to initial and boundary conditions the same as those proposed in [1]. The steady-state solution to equation (10) satisfies $\nabla\phi \cdot \nabla F = 0$, *i.e.* the variation of F along the normals to the level sets is null. The effect of the equation is thus to extend the force along the normals to the level sets.

3.1 Reinitialization

In principle, the level set function ϕ should be equal to the signed distance function from the zero level set throughout the contour evolution. In practice this is not true, and in order to correct the situation, reinitialization is required. Again to achieve maximum precision, we use the method proposed by Sussman and Fatemi in [34]. We thus solve the following partial differential equation for ψ, the reinitialized level set:

$$\psi_t = \text{sgn}(\phi)(1 - |\nabla\psi|) + \lambda(\psi) \ \ , \tag{11}$$

where the constraint functional λ is determined by the condition that, in each cell of the grid, the area inside the contour should be conserved. The aim is to prevent movement of the zero level set, which is a frequent side-effect of simpler reinitializations.

4 Application: line network detection

Automatic detection of line networks, and especially of road networks, in satellite imagery has been studied for the last fifteen years at least. Motivated by the increasing rate of data acquisition and the growing importance of geographic information systems, a wide variety of methods have been developed to attack this problem. Despite all this attention, extraction of line networks remains a challenge because of the great variability of the objects concerned, and the consequent difficulty in their characterization. The intensity of a road can vary significantly from one road to another, for example, while the presence of trees and buildings ('geometric noise') can obscure the network; junctions can be highly complex; networks do not possess exactly the same properties in rural and urban areas; and so on.

We mention briefly various methods that have been developed for the detection of line networks. Early methods used adapted operators such as edge detectors and morphological operations [30, 12]. Probabilistic methods using stochastic geometry and/or Markov random fields have been proposed [2, 35, 20]. Other methods minimize the optimal path between end points [9, 14]. Multi-scale approaches have been considered in [10]. Active contour models include 'ribbon snakes' [13, 21] and 'ziplock snakes' [24].

4.1 Energy Functional

There are two parts to any model, corresponding to the likelihood and the prior in probabilistic formulations: the prior terms, which do not mention the data, and the data terms, which do. Most models of road networks assume that the radiometry of a road is slowly varying and that there is significant contrast between roads and their environment, thus constraining the data term. They also assume that road width varies slowly with distance and that road curvature is small compared to inverse road width, except at intersections, thus constraining the prior terms.

The energy we will describe takes into account these generic properties, but also, through the presence of quadratic terms, other properties that are impossible to characterize with linear functionals, such as the fact that the roads form a network. The energy thus contains two parts:

$$E(C) = E_g(C) + \lambda E_i(C) \ \ , \tag{12}$$

where λ balances the contributions of the geometric part E_g and the data part E_i. The geometric part E_g is the sum of three terms, two linear (length and area), and one quadratic:

$$\begin{aligned} E_g(C) = &\oint dp\ \ |\vec{\mathbf{t}}| + \alpha\mathcal{A}(C) \\ &- \beta \oint\oint dp\, dp'\ \ \vec{\mathbf{t}} \cdot \vec{\mathbf{t}}'\ \Psi(R(p, p')) \ \ , \end{aligned} \tag{13}$$

where Ψ is defined in equation (7), $R(p, p')$ is the Euclidean distance between $C(p)$ and $C(p')$, and $\mathcal{A}(C)$ is the area of

the interior of the contour. The length term aims at minimizing the length of the contour and acts as a regularizing term. The area term is introduced to control the expansion of the fingered structure. It gives birth to a constant force in the direction of the inward normal. The effect of the quadratic term was discussed in section 2.

The image part E_i is composed of two terms:

$$E_i(C) = \oint dp\ \vec{\mathbf{n}} \cdot \nabla I - \oint \oint dp\, dp'\ \vec{\mathbf{t}} \cdot \vec{\mathbf{t}}'\ (\nabla I \cdot \nabla I')\ \Psi(R(p,p'))\ , \tag{14}$$

where $\vec{\mathbf{n}}$ is the unit outward normal to the contour. For clarity, we use primed and unprimed variables to designate quantities evaluated at points p (or $C(p)$) and p' (or $C(p')$) respectively.

The first data term favours situations in which the outward normal is opposed to the image gradient, or in other words, in which the road is lighter than its environment. When this is the case, it also favours larger gradients under the contour. The second term is an example of a quadratic data term: it describes a relation between the contour and the data that cannot be incorporated into a linear functional. Its effect is to favour situations in which pairs of points whose tangent vectors are anti-parallel and which are not too distant from each other (*i.e.* points on opposite sides of the road) lie on image gradients that point in opposite directions and are large.

The energy in equation (12) is minimized using gradient descent implemented via level sets as described in section 3. Thus the contour evolution is determined by

$$\frac{\partial C}{\partial t} = -\frac{\delta E}{\delta C}(C)\ , \tag{15}$$

where $\delta E/\delta C$ is the functional derivative of E with respect to C, *i.e.* it describes the change in energy δE due to a small change in the curve δC. The resulting equation of motion is then

$$\vec{\mathbf{n}} \cdot \frac{\partial C}{\partial t} = -\kappa - \lambda \nabla^2 I - \alpha + 2\lambda \oint dp'\ (\nabla I' \cdot \nabla \nabla I \cdot \vec{\mathbf{n}}')\ \Psi(R(p,p')) + 2 \oint dp'\ (\vec{\mathbf{R}} \cdot \vec{\mathbf{n}}')(\beta + \lambda \nabla I \cdot \nabla I')\ \Psi'(R(p,p'))\ , \tag{16}$$

where $\vec{\mathbf{R}} = (C(p) - C(p'))/|C(p) - C(p')|$. The component of $\partial C/\partial t$ along the normal has been taken, movement along the tangent direction being equivalent to a diffeomorphism of S^1, the domain of C, and thus irrelevant.

5 Experimental results

Ignoring the image terms completely, and evolving the contour under the influence of the prior, purely geometric terms, gives a good idea of the type of shapes favoured by the new energy. Classical linear energies evolve from an arbitrary shape towards a circle. If there is no area term, this circle will shrink and vanish. The presence of the area term will cause the circle to stabilize at a certain radius, where it will remain. In contrast, as discussed above, the minima of the quadratic energies are not circles. In fact, circles are unstable, "decaying" under evolution of the contour into, in our case, fingered shapes that are well adapted to line network extraction, demonstrating as they do elongated structures with parallel sides and slowly varying width.

In figure 2 are shown several evolutions based on the geometric terms E_g only. The parameter $d_{\min}$ of the Ψ function controls the minimum width of the fingers, and in the absence of data terms, all fingers collapse down to this limit. All the evolutions show the formation of fingered structures with parallel-sided arms of constant width. The first three rows of figure 2 show evolutions for different values of the parameter $d_{\min}$ that controls the width of the arms. We chose $d_{\min} = 3, 5, 7$; the fingers formed are of the correct width. The last two rows illustrate the role of the parameter α. In the fourth row $\alpha = 0.05$, while $\alpha = 0.1$ in the fifth row: the larger the value of α, the fewer the number of arms and the sparser the network.

We have also tested the above model on real satellite images. The results on two images are shown in figure 3. The images present several difficulties. There are regions of high gradient corresponding to the borders of fields rather than to roads. The fields are also objects with parallel sides. In the first image of figure 3, there is a discontinuity in the road. In both images, the roads are found.

Two important points need to be made here. The first concerns initialization. This is always an issue for gradient descent methods. The results may depend heavily on the initialization point, and indeed a number of methods used for the detection of roads rely on an initialization very close to the target. In contrast, we have found that starting from a rounded rectangle covering the greater part of the image domain is sufficient for the new energies. This is not surprising. Greater specificity in the prior term should eliminate many candidate contours from consideration, thus smoothing the energy surface, while at the same time deepening the minimum corresponding to the true network. The method should thus be less sensitive to initialization than less specific energies. The second point concerns termination. The results shown above are local minima of the energy: they evolve no further under more iterations.

Figure 4 shows another result. It is quite good, but the errors it contains illustrate some of the outstanding issues with the model. There is a piece of contour remaining that does not correspond to a road, and the road to the bottom right has not extended far enough. There is also a gap in the road at the junction.

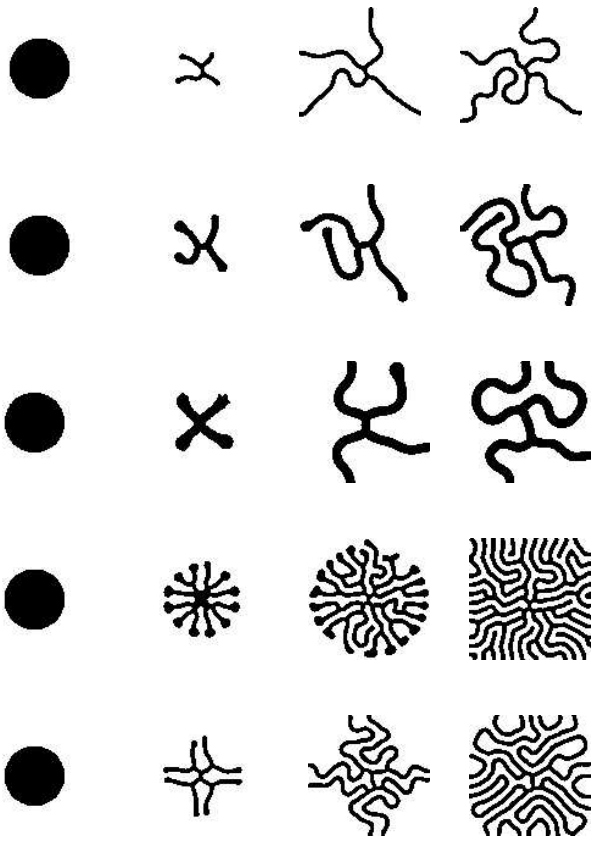

Figure 2: Geometrical evolutions for different values of the parameter $d_{\min}$ (first three rows) and α (last two rows).

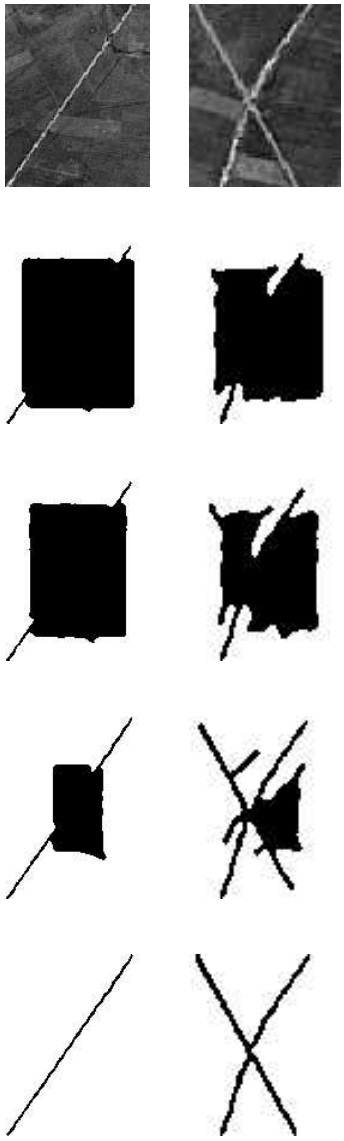

Figure 3: Detection of roads in 2 satellite images.

6 Conclusions

We have introduced a new class of active contour energy functionals. These energies are quadratic on the space of one-chains, in contrast to classical energies, which are linear. The new energies enable us to introduce complex geometrical information into the model. We studied a particular form of quadratic energy whose minima consist of fingered structures with parallel sides. We can control the width and the number of arms formed. Using this energy as a base, we designed an energy functional for the detection of roads in satellite imagery and tested it on real satellite images. Simulations prove the efficiency of the model and illustrate the effect of the incorporation of non-trivial geometrical interactions between points of the contour. Algorithmically, these models presented new challenges, in particular the need for a maximum of precision in the calculation of the force and the evolution of the contour.

Immediate future work is focused on the solution of the problems mentioned in connection with figure 4. We are designing a quadratic 'gap closure' force that will overcome the repulsion introduced by the existing quadratic term in certain special circumstances. This force will also help to eliminate small remnant areas. We are also developing the existing quadratic term so that it encourages road extensions even more than it does at present.

It is clear that the use of higher-order energies is not limited to line network detection in remote sensing data. One obvious application of the models presented here is to biological and medical imagery, where the geometry required is often similar.

We are only just beginning to explore the modelling possibilities of quadratic energies. Many open questions and research directions (*e.g.* higher-than-quadratic functionals; extension to surfaces; probabilistic formulation and the link to field theory; parameter and model estimation; new level set techniques; computational efficiency) remain to be explored.

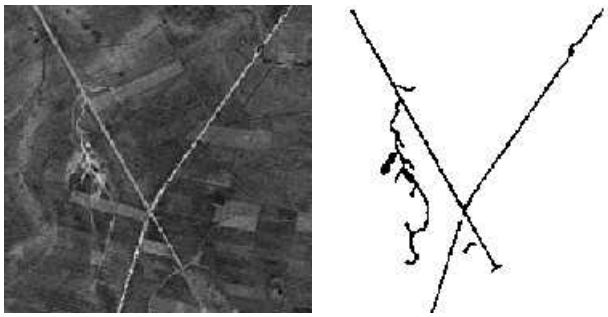

Figure 4: Result on a larger image

References

[1] D. Adalsteinsson and J. A. Sethian. The fast construction of extension velocities in level set methods. *J. Comp. Phys.*, 148:2–22, 1999.

[2] M. Barzohar and D. B. Cooper. Automatic finding of main roads in aerial images by using geometric-stochastic models and estimation. *IEEE Trans. PAMI*, 18(2):707–721, 1996.

[3] V. Caselles, F. Catte, T. Coll, and F. Dibos. A geometric model for active contours. *Numerische Mathematik*, 66:1–31, 1993.

[4] V. Caselles, R. Kimmel, and G. Sapiro. Geodesic active contours. *IJCV*, 22(1):61–79, 1997.

[5] T. F. Chan and L. A. Vese. Active contours without edges. *IEEE Trans. IP*, 10(2):266–277, 2001.

[6] Y. C. Chang, T. Y. Hou, B. Merriman, and S. Osher. A level set formulation of Eulerian interface capturing methods for incompressible fluid flows. *J. Comp. Phys.*, 124:449–464, 1996.

[7] Y. Chen, S. Thiruvenkadam, H. D. Tagare, F. Huang, D. Wilson, and E. A. Geiser. On the incorporation of shape priors into geometric active contours. *Proc. IEEE Workshop VLSM*, pages 145–152, 2001.

[8] L. D. Cohen. On active contours and balloons. *CVGIP: Image Understanding*, 53:211–218, 1991.

[9] J. M. Coughlan and A. L. Yuille. Bayesian A* tree search with expected o(n) convergence rates for road tracking. *Proc. EMMCVPR*, 1654:189–204, 1999. Springer-Verlag.

[10] I. Couloigner. *Reconnaissance de Formes dans des Images de Télédétection du Milieu Urbain*. PhD thesis, UNSA, 1998.

[11] D. Cremers, C. Schnorr, and J. Weickert. Diffusion-snakes: combining statistical shape knowledge and image information in a variational framework. *Proc. IEEE Workshop VLSM*, pages 137–144, 2001.

[12] M. A. Fischler, J. M. Tenenbaum, and H. C. Wolf. Detection of roads and linear structures in low-resolution aerial imagery using a multisource knowledge integration technique. *Comp. Graph. and Image Processing*, 15:201–223, 1981.

[13] P. Fua and Y. G. Leclerc. Model driven edge detection. *Mach. Vis. and Appl.*, 3:45–56, 1990.

[14] D. Geman and B. Jedynak. An active testing model for tracking roads in satellite images. *IEEE Trans. PAMI*, 18:1–14, 1996.

[15] S. Jehan-Besson, M. Barlaud, and G. Aubert. Dream^{2}s: Deformable regions driven by an eulerian accurate minimization method for image and video segmentation. *IJCV*, 2003. To appear.

[16] I. H. Jermyn. On Bayesian estimation in manifolds. Technical Report 4607, INRIA, 2003.

[17] I. H. Jermyn and H. Ishikawa. Globally optimal regions and boundaries as minimum ratio weight cycles. *IEEE Trans. PAMI*, 23(10):1075–1068, 2001.

[18] M. Kass, A. Witkin, and D. Terzopoulos. Snakes: Active contour models. *IJCV*, 1(4):321–331, 1988.

[19] S. Kichenassamy, A. Kumar, P. Olver, A. Tannenbaum, and A. Yezzi. Gradient flows and geometric active contour models. *Proc. IEEE ICCV*, pages 810–815, 1995.

[20] C. Lacoste, X. Descombes, and J. Zerubia. A comparative study of point processes for line network extraction in remote sensing. Technical Report 4516, INRIA, 2002.

[21] I. Laptev, T. Lindeberg, W. Eckstein, C. Steger, and A. Baumgartner. Automatic extraction of roads from aerial images based on scale space and snakes. *Mach. Vis. and Appl.*, 12:23–31, 2000.

[22] M. E. Leventon, W. E. L. Grimson, and O. Faugeras. Statistical shape influence in geodesic active contours. *Proc. IEEE CVPR*, 1:316–322, 2000.

[23] R. Malladi, J. A. Sethian, and B. C. Vemuri. Shape modeling with front propagation: A level set approach. *IEEE Trans. PAMI*, 17(2):158–175, 1995.

[24] W. M. Neuenschwander, P. Fua, L. Iverson, G. Székely, and O. Kubler. Ziplock snakes. *IJCV*, 25(3):191–201, 1997.

[25] S. Osher and J. A. Sethian. Fronts propagating with curvature dependent speed: Algorithms based on Hamilton-Jacobi formulations. *J. Comp. Phys.*, 79:12–49, 1988.

[26] N. Paragios and R. Deriche. Geodesic active regions: A new framework to deal with frame partition problems in computer vision. *J. Vis. Comm. and Image Repr.*, 13:249–268, 2002.

[27] N. Paragios and M. Rousson. Shape priors for level set representations. *ECCV*, pages 78–92, 2002.

[28] D. Peng, B. Merriman, S. Osher, H. Zhao, and M. Kang. A PDE-based fast local level set method. *J. Comp. Phys.*, 155:410–438, 1999.

[29] M. Rochery, I. H. Jermyn, and J. Zerubia. Étude d'une nouvelle classe de contours actifs pour la détection de routes dans des images de télédétection. In *Proc. GRETSI*, Paris, France, September 2003.

[30] M. A. Serendero. *Extraction d'Informations Symboliques en Imagerie SPOT: Réseaux de Communication et Agglomérations*. PhD thesis, UNSA, 1989.

[31] J. A. Sethian. Fast marching methods. *SIAM Rev.*, 41(2):199–235, 1996.

[32] J. A. Sethian. *Level Set Methods and Fast Marching Methods: Evolving Interfaces in Geometry Fluid Mechanics, Computer Vision and Materials Science*. CUP, 1999.

[33] K. Siddiqi, B. B. Kimia, and C-W. Shu. Geometric shock-capturing ENO schemes for subpixel interpolation, computation and curve evolution. *Graphical Models and Image Processing*, 59:278–301, 1997.

[34] M. Sussman and E. Fatemi. An efficient, interface-preserving level set redistancing algorithm and its application to interfacial incompressible fluid flow. *SIAM J. Sci. Comp.*, 20(4):1165–1191, 1997.

[35] F. Tupin, H. Maitre, J-F. Mangin, J-M. Nicolas, and E. Pechersky. Detection of linear features in SAR images: Application to road network extraction. *IEEE Trans. Geoscience and Remote Sensing*, 36(2):434–453, 1998.